Virology 414 (2011) 51–62

Contents lists available at ScienceDirect

Virology

journal homepage: www.elsevier.com/locate/yviro

Importance of viral genomic composition in modulating glycoprotein content on the surface of influenza virus particles

Vincent Moulès [a,*,1], Olivier Terrier [a,b,*,1], Matthieu Yver [a], Beatrice Riteau [a,c], Christine Moriscot [d,e], Olivier Ferraris [a], Thomas Julien [a], Emmanuel Giudice [f], Jean-Paul Rolland [f], Alexandra Erny [a], Maude Bouscambert-Duchamp [a,g], Emilie Frobert [a,g], Manuel Rosa-Calatrava [a], Yi Pu Lin [h], Alan Hay [h], Daniel Thomas [f], Guy Schoehn [d,e], Bruno Lina [a,g]

[a] Université Lyon 1, Faculté de médecine RTH Laennec, CNRS FRE 3011 VirPath, Virologie et Pathologie Humaine, F-69008 Lyon, France
[b] Division of Medical Sciences, Center for Oncology and Molecular Medicine, Dundee University, Ninewells Hospital and Medical School, Dundee, DD1 9SY, UK
[c] INRA, Département de Santé Animale, Tour-Nouzilly, France
[d] CEA-CNRS-Université J. Fourier Institut de Biologie Structurale UMR 5075 41 rue Jules Horowitz 38 027 Grenoble Cedex 1, France
[e] Université J. Fourier—EMBL—CNRS Unit for Virus Host Cell Interactions, UMI 3265 6, rue Jules Horowitz, 38042 Grenoble, France
[f] Université Rennes 1, CNRS Interactions Cellulaires et Moléculaires, UMR 6026, Campus de Beaulieu, bâtiment 13, F-35042 Rennes Cedex, France
[g] Laboratoire de Virologie, Centre de Biologie et de Pathologie Est, Hospices Civils de Lyon, 59, Boulevard Pinel, 69677 Bron cedex, France
[h] Virology Division, MRC National Institute for Medical Research, The Ridgeway, London NW7 1AA, UK

ARTICLE INFO

Article history:
Received 14 January 2011
Returned to author for revision
24 February 2011
Accepted 14 March 2011
Available online 5 April 2011

Keywords:
Influenza
Orthomyxoviridae
Viral glycoprotein
Haemagglutinin (HA)
Neuraminidase (NA)
Cryo-electron microscopy (cryo-EM)

ABSTRACT

Despite progress in our knowledge of the internal organisation of influenza virus particles, little is known about the determinants of their morphology and, more particularly, of the actual abundance of structural proteins at the virion level. To address these issues, we used cryo-EM to focus on viral (and host) factors that might account for observed differences in virion morphology and characteristics such as size, shape and glycoprotein (GP) spike density. Twelve recombinant viruses were characterised in terms of their morphology, neuraminidase activity and virus growth. The genomic composition was shown to be important in determining the GP spike density. In particular, polymerase gene segments and especially PB1/PB2 were shown to have a prominent influence in addition to that for HA in determining GP spike density, a feature consistent with a functional link between these virus components important for virus fitness.

Introduction

Influenza viruses belong to the *Orthomyxoviridae* family of enveloped viruses with segmented genomes of single-stranded negative sense RNA (Lamb and Krug, 2001). Among the three types of influenza (A, B and C), type A viruses are the most virulent pathogens and cause most severe disease. They exhibit a wide antigenic diversity represented by combinations of 16 HA and 9 NA subtypes and a broad host range. Two subtypes have recently circulated in the human population, A(H3N2) and A(H1N1). The recent emergence of the 'swine' A(H1N1) 2009 virus that spread to cause a human pandemic, posed major challenges to the public health sector and the scientific communities worldwide (Neumann et al., 2009).

The influenza virion contains eight helical ribonucleocapsids, also called viral ribonucleoproteins (vRNPs), each encoding structural proteins. The RNPs are composed of single stranded RNA which is tightly and regularly encapsidated by viral nucleoprotein (NP). Each vRNP is associated with a heterotrimeric polymerase (PA/PB1/PB2) (Palese and Shaw, 2007). The viral envelope consists of a lipid bilayer containing three transmembrane proteins: haemagglutinin (HA), neuraminidase (NA) and M2 (ion channel). The matrix (M1) protein is thought to underlie the lipid bilayer, which is derived from the host cell plasma membrane containing lipid rafts or non-lipid rafts of varying composition depending on cellular origin (Zhang et al., 2000).

The HA, the major envelope protein, is a trimeric spike possessing the binding sites for sialo-conjugate receptors. As a class I viral fusion protein, the HA has two major functions: attachment to cellular receptors and membrane fusion (Skehel and Wiley, 2002), and it possesses the principal epitopes for neutralising antibodies. The second most abundant transmembrane protein, the tetrameric NA, is responsible for the cleavage of cell surface receptors and plays a

* Corresponding authors.
E-mail addresses: vincent.moules@univ-lyon1.fr (V. Moulès), olivierterrier@me.com (O. Terrier).
[1] Authors VM and OT contributed equally to this work

0042-6822/$ – see front matter © 2011 Elsevier Inc. All rights reserved.
doi:10.1016/j.virol.2011.03.011

critical role in the release of progeny virions. This sialidase activity can vary among influenza strains due to intrinsic properties of the NA and the amounts of NA on the surface of virions (Gong et al., 2007).

Two licenced anti-influenza drugs, zanamivir and oseltamivir, act by inhibiting the neuraminidase activity, thereby reducing replication both *in vitro* and *in vivo*. Whereas mutations in the NA have been responsible for drug resistance *in vivo*, compensatory mutations on the HA, which reduced the efficiency of virus binding to sialic acids and consequently decreased dependence on NA function, have caused drug resistance *in vitro* (Gubareva et al., 1996; McKimm-Breschkin et al., 1996; Staschke et al., 1995). The functional balance between HA and NA proteins is therefore thought to be critical for optimal replication and dissemination of the virus.

The allantoic cavity of embryonated chicken eggs is the substrate widely used for production of inactivated influenza vaccines, usually using reassortant viruses containing the internal genes of the A/Puerto Rico/8/34(PR8, H1N1) strain, which confer high growth in eggs, together with the genes encoding the surface antigens of the current influenza A (epidemic/pandemic) strain (Lamb and Krug, 2001).

Analyses of virion structure have provided important information about the processes of virus morphogenesis and budding (see Nayak et al., 2009 for review). Moreover, the architecture and morphology of virus particles are of interest not only in the context of virus assembly but also in light of the possibility that pleiomorphic variation may correlate with differences in infectivity and/or pathogenicity (Harris et al., 2006). To date, the morphology of influenza viruses has been based mainly on transmission electron microscopy (TEM) of negatively stained samples or thin sections of infected cells (Hayase et al., 1995; Ruigrok et al., 1984); however, sample preparation may introduce morphological artefacts, as has been shown for influenza and other enveloped viruses, such as PIV-5 (Ruigrok et al., 1992; Terrier et al., 2009). In contrast, cryo-electron microscopy (cryo-EM) of ice-embedded virions maintains the virus structure in a natural hydrated state and has allowed the acquisition of more accurate data on the influenza virus structure (Booy et al., 1985; Fujiyoshi et al., 1994). More recently, both cryo-EM and cryo-electron tomography (cryo-ET) have been successfully used to analyse the structure of different enveloped viruses, including paramyxoviruses and bunyaviruses (Calder et al., 2010; Huiskonen et al., 2009; Loney et al., 2009; Sherman et al., 2009; Terrier et al., 2009).

Using cryo-ET, Harris et al. (2006) analysed the detailed structure of ice-embedded recombinant X31(H3N2) virions, which were grown in embryonated eggs. That study revealed a relatively low level of virus pleiomorphism (80% spheroidal) and the presence of around 300 HA and 40 NA spikes on the surface of an average 120 nm virion, with some clustering of NA in certain areas (Harris et al., 2006). Also using cryo-ET, Nayak et al. (2009) studied the A(H1N1) viruses, A/PR/8/34 and A/WSN/33, grown in MDCK cells, yielding similar results to those of Harris et al., despite apparent specific differences in morphological features. These more recent studies have added interesting and complementary data to previous work on the organisation of vRNPs within virus particles and provide further support for a specific mechanism of vRNP incorporation (Noda et al., 2006). To complete the characterization of naturally occurring NA-minus H3 (H3NA-) viruses, we recently performed a cryo-EM study on the H3N2 virus A/California/7/04 grown in MDCK cells (Moules et al., 2010). Interestingly, our results indicated a more heterogeneous morphology and a greater number of surface glycoproteins, of around 400–500, than described by Harris et al. (2006), closer to that determined previously for an influenza B virus by scanning electron microscopy (Ruigrok et al., 1984). Despite progress in our understanding of the internal organisation of influenza virus particles, little is known about the factors which determine their morphology or the actual abundance of structural proteins at the virion level and only a few studies have been dedicated to these aspects of influenza biology.

To address this issue, we have used cryo-EM to study the influence of viral and host factors on influenza virus morphology and characteristics such as size, shape and glycoprotein (GP) spike density. Based on the differences observed between viruses of the H3N2 and H1N1 subtypes, notably in terms of GP spike surface densities, we constructed, using reverse genetics, 12 recombinant influenza viruses with different combinations of gene segments from viruses of the two subtypes, in order to evaluate the influence of genomic composition. These recombinant viruses were characterised structurally and as regards certain features of their replication *in vitro*. Our results indicate a prominent role for polymerase gene segments, especially PB1, in addition to that for HA, in determining GP spike density, with possible influence on the HA/NA ratio and replicative fitness.

Results

Our initial observations from cryo-EM analysis of influenza viruses differed in certain respects from published data, in terms of pleiomorphy and apparent GP surface density. However, in most cases, neither the same virus (type, subtype or strain) nor the same experimental conditions (e.g. purification and observation techniques) were used. In order to obtain a more precise view of the morphological features of influenza virus with a comparable set of data, in this study we used the same purification and observation protocols to compare several batches of two human virus subtypes and recombinants of various genomic compositions.

Comparison of morphological features between H1N1 and H3N2 viruses

Using cryo-EM, we studied virions embedded in vitreous ice in preparations of A/NewCaledonia/20/99(H1N1) and A/California/7/04 (H3N2) viruses, purified from infected MDCK cell supernatants, using identical protocols, as indicated in Materials and methods (Fig. 1A, two upper vignettes). We scanned a large part of the grid and every particle observed was imaged. All particles were observed to be covered with glycoprotein spikes protruding from the virion surface. We first classified the virions in terms of shape into three groups based on axial ratios. Viruses with axial ratio ranges of 1.0–1.2, 1.2–1.6 and >1.6 were classified respectively as spherical, spheroidal and elongated (Fig. 1B). We chose not to use the classification previously proposed by Harris et al. (2006) since it is adapted more to cryo-ET, and the matrix and internal organisation are not easily visible by our cryo-EM approach. The A/NewCaledonia/20/99(H1N1) virus comprised only spherical particles (100%, $n=23$), whereas the A/California/7/04(H3N2) virus was comprised of similar proportions of the three categories of particle shape, with 38.0% ($n=11$) spherical particles, 34.5% spheroidal ($n=10$) and 27.5% elongated ($n=8$) (Fig. 1B). We also noted that the spherical particles of the H1N1 virus had a larger diameter than those of the H3N2 virus (Supplementary Fig. 1). These results were in reasonable agreement with previously published data as regards virus particle shape (Booy et al., 1985; Calder et al., 2010; Fujiyoshi et al., 1994; Harris et al., 2006).

Despite difficulties in clearly identifying the ultrastructure of the spike GPs and potentially discriminating HA from NA, it was possible to count them. Indeed, the GP spike stalks were easily distinguishable at the edge of the projected image of the virus between the lipid bilayer and the electron opaque layer formed by the GP globular heads (Fig. 1A). Harris et al. (2006) have shown that some GP clustering exists on the virus surface. In our cryo-EM images we obtained projections of virus particles which showed that the number of GP at the edge of the virion could vary depending on the orientation of the particle. To limit the influence of uneven distribution of spikes on the virus surface we analysed more than 14 virus particles of each type. The relatively low SD obtained in all cases suggested that clustering was infrequent and that the distribution of GP on the virus surface was quite uniform.

For the H1N1 virus, the spacing between 4 GP spike stalks was measured as 31.1 +/− 1.3 nm ($n=28$, Fig. 1C). From these data we estimated a surface GP number ranging between 478 and 566 for a

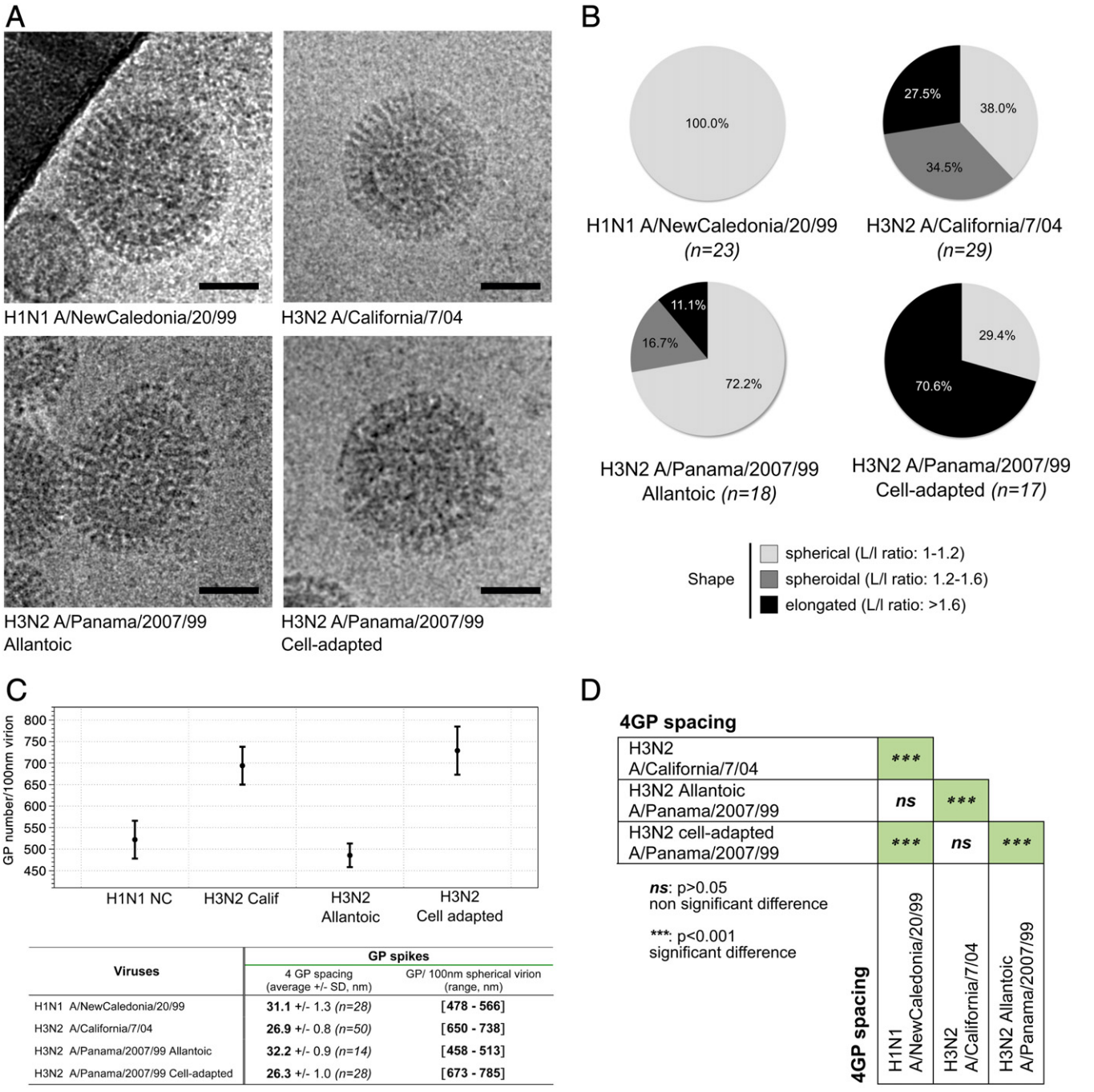

Viruses	GP spikes	
	4 GP spacing (average +/- SD, nm)	GP/ 100nm spherical virion (range, nm)
H1N1 A/NewCaledonia/20/99	**31.1** +/- 1.3 *(n=28)*	**[478 - 566]**
H3N2 A/California/7/04	**26.9** +/- 0.8 *(n=50)*	**[650 - 738]**
H3N2 A/Panama/2007/99 Allantoic	**32.2** +/- 0.9 *(n=14)*	**[458 - 513]**
H3N2 A/Panama/2007/99 Cell-adapted	**26.3** +/- 1.0 *(n=28)*	**[673 - 785]**

Fig. 1. Comparison of morphological features between human influenza A subtypes by cryo-electron microscopy. A. Representative micrographs of ice-embedded A/NewCaledonia/20/99(H1N1) and A/California/7/04(H3N2) virions, both grown in MDCK cells (two upper vignettes). Two micrographs of a similar H3N2 strain, A/Panama/2007/99, are shown, one exclusively cultivated in the allantoic cavity of embryonated chicken eggs and the other following four additional passages in MDCK cells (two lower vignettes). Scale bars: 50 nm. B. Proportions of the different shapes observed for the four different viruses, the total number of virions analysed for each virus is indicated in brackets. C. Measures of the 4GP spacing for each virus and determination of the surface GP range per 100 nm diameter virion. An example of the calculation is given in Supplementary Fig. 2. D. Dunn's multiple comparisons test, after a non-parametric ANOVA (Kruskal–Wallis test). Statistical analysis is based on 4GP-spacing data obtained from the four different influenza viruses.

100 nm diameter virion (Fig. 1C and Supplementary Fig. 2 for an example of the calculation). For the H3N2 virus, the same measurement revealed a spacing of 26.9 +/− 0.8 nm ($n=50$) and an estimated surface GP number ranging between 650 and 738 for a 100 nm diameter virion, indicating a 23%–26% increase in GP number compared to that for the H1N1 A/NewCaledonia/20/99 virus (Fig. 1C). This 4GP-spacing measurement, reflecting GP surface density, was significantly different ($p<0.001$) between the two viruses (Fig. 1D). Considering the pleiomorphism, we also showed that there was no statistical difference in the average inter-GP spacing between the different shape classes (data not shown).

Interestingly, these initial observations were in agreement with an earlier description by Ruigrok et al. but were not in complete accordance with other available published data, particularly in terms of the surface GP density (Inglis et al., 1976; Ruigrok et al., 1984). Differences from our study included both the mode of virus production (allantoic cavity of chicken eggs versus MDCK cells) and the virus strain.

To investigate the possible influence of cell substrate on the GP spike density, we analysed a contemporary H3N2 virus, A/Panama/2007/99, produced in either egg or cell culture (4 additional passages in MDCK cells) (Fig. 1A, lower two vignettes). The proportions of different particle shapes were quite different, with a majority of spherical virions for the egg-derived virus (72.2%, $n=13$) and a majority of elongated virions for the cell culture-derived virus (70.6%; $n=12$) (Fig. 1B). In addition, the surface GP densities differed according to the mode of production (Fig. 1C). The surface GP number ranges were estimated to be 458–513 and 673–785, respectively, for egg-derived and cell culture-derived 100 nm diameter virions, representing a marked difference of 31%–34% (Fig. 1C). Statistical analysis of the 4GP spacing measurements indicated significant differences ($p<0.001$) between the two A/Panama/2007/99 virus preparations, but no significant difference between the two cell culture-derived H3N2 viruses, A/California/7/04 and A/Panama/2007/99 (Fig. 1D). Sequence analyses showed that there was no change in the HA or NA of the A/Panama/2007/99 virus as a result of passage in cell culture, which might have contributed to the morphological differences (data not shown).

In summary, these observations indicate an influence of both the virus subtype and the mode of virus production, *i.e.* the cellular substrate, on virion morphological features and especially the density of GP.

Comparison of morphological features between recombinant H1N1 and H3N2 viruses

The results obtained for the egg-derived A/Panama/2007/99 (H3N2) virus were quite different with those previously described for the egg-derived H3N2 X31 reassortant virus (Harris et al., 2006), with a greater than 25%–34% difference in the total number of GPs at the virion surface. Considering the particular origin of the different gene segments of the X31 strain, which possessed six 'internal' gene segments of PR8, we hypothesised that the genomic composition may contribute to morphological features and thus investigated its influence on surface GP number using reverse genetics.

In order to validate our approach, an initial morphological analysis was carried out on the recombinant 'parental' viruses, A/Puerto Rico/8/34(H1N1) (PR8) and A/Moscow/10/99(H3N2) (MO), obtained by reverse genetics. We found a similar shape distribution between recombinant MO and the natural H3N2 isolates (Figs. 1 and 3). The proportion of spherical, spheroidal and elongated virions were respectively 40% ($n=18$), 28.9% ($n=13$) and 31.1% ($n=14$) for MO and 51.2% ($n=21$), 0% ($n=0$) and 48.8% ($n=20$) for PR8 viruses (Fig. 3B). Differences were therefore observed between the recombinant PR8 virus and the recent natural H1N1 virus isolate (Figs. 1B and 3B). The spherical particles of PR8 and MO had similar average diameters of respectively 94.2 +/− 15.4 nm and 96.0 +/− 12.2 nm, close to those measured for the natural isolates (Supplementary Fig. 1).The GP number for a 100 nm diameter virion was estimated to be in the range of 477–527 for PR8 and 656–738 for MO virions (Fig. 5A). The significant difference in the surface GP number observed between the two subtypes was maintained in the recombinant viruses, with over 27%–28.5% more GPs on the MO virus. Statistical analysis indicated that the 4GP spacing averages were significantly different between PR8 and MO ($p<0.001$) (Fig. 5B). We also observed no statistically significant differences between natural isolates and recombinant strains of the same subtype (Supplementary Fig. 3) and confirmed that no differences existed between the different shape classes for each virus (data not shown).

In conclusion, these analyses revealed that the GP spike densities were statistically different between the recombinant H1N1 and H3N2 viruses and correlated with the differences observed between the non-recombinant viruses of H1N1 and H3N2 subtypes.

To assess the influence of different gene segments on the GP surface density, we produced a series of ten recombinant viruses, A–J, composed of different gene constellations from PR8 and MO viruses (Fig. 2). The genetic compositions of viruses A–E typically correspond to those of vaccine viruses, with MO H3 and N2 (B–E plus a third MO) gene segments on a variable PR8 genetic background. Viruses G and H possess only the MO H3 or N2 gene segment, while viruses F, I and J all possess the MO PB1 segment with or without MO N2 or MO H3 segments on a PR8 genetic background (Fig. 2).

Using cryo-EM, we studied the morphology of each recombinant virus (Fig. 3A) and recorded data on particle shape in Fig. 3B (data concerning particle size are compiled in Supplementary Fig. 1). Interestingly, for all the recombinant viruses observed ($n=266$), more than 67% ($n=179$) were classified as elongated; with the exception of viruses I and J, all presented more than 60% of elongated particles, greater than that measured for PR8. By comparing viruses A, B and C, we observed that whereas the introduction of the additional MO M gene segment was associated with a reduction (more than 15%) in elongated forms, the introduction of the additional MO NS gene segment was associated with a complete absence of spherical or spheroidal forms (Fig. 3B). Overall however, no clear relationship between particle shape and genomic composition could be easily discerned and the genomic composition might not be the only determinant of virus size and shape.

Comparisons with PR8 and MO strains as reference revealed two main groups of recombinants based on the average GP number/100 nm virion. The first, Group I "PR8-like," contains viruses A, B, C and G and the second, group II "MO-like," viruses D, E and F, with viruses H, I and J showing characteristics intermediate between the two groups (Fig. 4). Analyses of the genomic compositions of the different viruses revealed that only certain combinations of MO gene segments on a PR8 genetic background correlated with a group II "MO-like" phenotype. Among viruses A–F, only the combinations of MO PB1 or MO PB2 with MO H3 and/or N2 (viruses D–F) were associated with a high GP number range, similar to that measured for MO (Fig. 5A). This association was confirmed by statistical analysis which showed that there was no significant difference ($p>0.05$) between MO and viruses D, E and F in terms of GP spacing (Fig. 5B). In contrast, a significant difference ($p<0.001$) was observed between H3N2 MO and viruses A, B and C. The reciprocal statistical analysis between PR8 and viruses A–F was also conclusive (Fig. 5B). Data obtained for viruses G–J gave additional information on the nature and complexity of the association between gene segment combination and "MO-like" phenotype: a MO HA, NA or PB1 encoding gene segment alone in a PR8 genetic background (viruses G, H and J) did not produce a GP number range equivalent to that estimated for MO (Figs. 4B and 5A). A statistical comparison of 4GP spacing measurements between viruses G–J and MO revealed a significant difference ($p<0.001$). The reciprocal statistical analysis between the same viruses and PR8 also revealed significant differences for H (MO NA

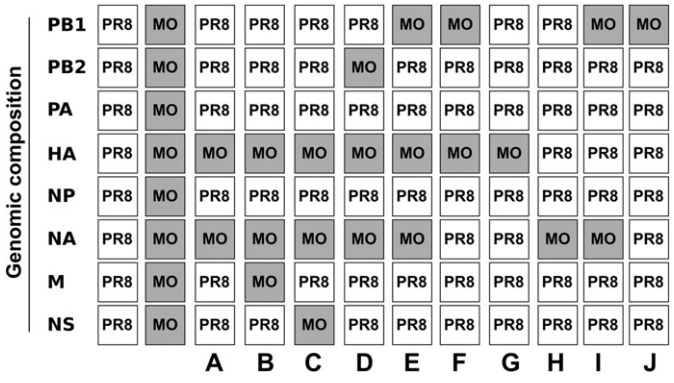

Fig. 2. Genomic composition of 12 different influenza viruses obtained by reverse genetic.

only, $p<0.01$) and J (MO PB1 only, $p<0.001$), but not for viruses G (MO HA only, $p>0.05$) and I (MO PB1 and NA, $p>0.05$) (Fig. 5B). Altogether, the results indicate that the combination of HA and PB1 or PB2 MO gene segments on a PR8 genetic background correlates with a high surface GP number. Our goal was not to analyse all the possible combinations of MO and PR8 gene segments, the number of recombinant viruses to construct, purify and observe being too large (theoretically $n=256$).

This first analysis has highlighted the important yet non-exclusive role of the genetic background in determining the surface GP spike density of influenza viruses.

Characterisation of the NA activity of the recombinant viruses

Our results strongly support the genomic composition having an impact on the surface GP density of recombinant viruses; however, its possible impact on the NA quantity remains to be investigated. Based on the approximation that 50–100 NA molecules are incorporated into each virion, neuraminidase activity has been used to quantify the amount of virus (Nayak and Reichl, 2004). Recently, using a fluorescent substrate (MU-NANA), Eichelberger et al. (2008) showed a proportional relationship between NA activity and influenza virus titer (TCID50) from 0 to 10E5 TCID50/50 µl. To test the impact of the genomic composition on the incorporation of N1 or N2 proteins into the viral membrane, we determined the NA activity (RFU) for each of the recombinant viruses (at 10E5 TCID50/50 µl) following 1 h of incubation with the fluorescent substrate (MUNANA) (Fig. 6). Moreover, we verified that the incorporation of N1 or N2 proteins into the different genetic backgrounds did not change their enzymatic characteristics by confirming unchanged Michaelis–Menten constants (Km) (data not shown). As the same quantity of infectious virus was used in each case, with an unchanged Km, we have used differences in the rate of enzyme reaction as an estimate of different extents of incorporation of NA molecules into each virus.

Determination of RFU for the 7 recombinant viruses harbouring the N2 coding sequence distinguished two groups: the first (viruses A, B, C, D, H and I) gave RFU that were 1–2 fold lower than that measured for MO, while the second group (virus E) gave RFU twice that measured for virus MO (Fig. 6). For recombinant viruses possessing N1, viruses F and J gave a 2–5 fold higher RFU, respectively, than PR8, while recombinant G virus had a slightly reduced RFU (Fig. 6). Most notable were the increases due to replacement of PR8 PB1 by that of MO. Comparisons of J vs PR8, F vs G and E vs A shows that the switch in PB1 causes an approximate 4-fold increase in RFU for NA. In each case there was a corresponding increase in GP number. However, the switch in PB2 (recombinant D virus) causes an approximate 2-fold decrease in RFU for NA, though an increase in GP number (Fig. 6).

In the absence of more definitive measurements of the ratio of NA: HA GP spikes, these results suggest that the genetic determinants of GP spike density may also influence the ratio of the two GP spikes on the virus particle.

Kinetics of replication in vitro of recombinant viruses

To investigate whether there is any relationship between GP spike density, and possible modulation of the HA/NA ratio, and virus growth capacity, we compared the growth kinetics of the recombinant viruses by infecting both MDCK and MDCK-SIAT1 cells at a MOI of 10^{-4} and monitoring the release of infectious virus progeny up to 48 hpi (Fig. 7B). MDCK-SIAT1 cells, that stably over-express the human α2-6 sialyltransferase, have proved to be a more suitable system than MDCK cells to monitor the effects of changes in HA/NA ratio on the virus growth cycle (Matrosovich et al., 2003; Moules et al., 2010). As already observed with viruses resistant to neuraminidase inhibitors, modification of growth properties in MDCK-SIAT1 cells are associated with a modulation of the functional HA/NA balance (Moules et al., 2010).

As shown in Fig. 7, the infectivity in the supernatant of MDCK cells infected with recombinant viruses increased exponentially and reached a maximum titer of approximately 8 logs TCID50/ml at 48 hpi, with relatively little difference between the viruses. Significant differences were, however, observed in the titers at 48 hpi between MDCK and MDCK-SIAT1 cells infected by recombinants B, D, E, F and H (Fig. 7A). In MDCK-SIAT1 infected cells, titers at 48 hpi were about 2 and 4 log lower, respectively, for D and H, and for B, E and F recombinant viruses, compared to MO virus (Fig. 7A). However, whereas growth was generally slower over the 48 h for viruses E and F, both of which possessed PB1 and HA of MO, titers of B, D and H were not reduced at 24 h but subsequently increased to a lesser extent in MDCK-SIAT1 cells than in MDCK cells (Fig. 7B). Of the recombinant viruses with higher NA activity, those possessing the H3 protein (viruses E and F) replicated to lower titre in MDCK-SIAT1 cells than that harbouring the H1 protein (virus J).

These results suggest that variations of virus production in MDCK-SIAT1 cells might be a consequence of modulation of the HA/NA functional balance. Moreover, these data highlight a potential impact of the genome constellation on the HA/NA ratio at the viral surface.

Discussion

Despite the growing interest in influenza viruses stimulated by the pandemic threat of highly pathogenic avian H5N1 and the recent H1N1 pandemic, little is known about many facets of their biology. The initial aim of our study was to obtain further understanding of the morphological determinants of influenza viruses and indirectly gain information about the processes of morphogenesis and budding. Recent technological developments in electron microscopy, notably in cryo-EM and cryo-ET, have enabled the examination of the structure of viruses in their 'natural' state, eliminating a major source of artifactual observations (Calder et al., 2010; Harris et al., 2006; Nayak et al., 2009; Yamaguchi et al., 2008). Studies of influenza viruses, using these more powerful techniques, have focused on a limited number of different viruses produced in different cell substrates (MDCK cells or chicken eggs) with differences in the purification protocols. They have revealed a marked heterogeneity in terms of size and shape among the viruses examined, both in relation to the cellular host and the particular virus strain (Harris et al., 2006). In order to enhance and complement these observations and avoid technical variation as much as possible, we have used a single cell substrate, purification and observation procedure to examine a set of natural and recombinant influenza viruses of the human H1N1 and H3N2 subtypes. To our knowledge, this is the first time that reverse genetics techniques have been used in a cryo-EM study of the influenza virion.

Our results showed that viruses of the two subtypes present differences both in terms of the relative proportions of different shapes and surface GP densities. Indeed our observations revealed that, for virions of equal diameter, the H3N2 viruses harboured a significantly higher number of GP spikes (more than 24%) than the H1N1 viruses, both in their 'natural' and genetic-engineered states. The proportions of different shapes and GP densities were well conserved between A/California/7/04 and the genetic-engineered A/Moscow/10/99 H3N2 strains. In contrast, although they shared a similar GP density, the reverse genetic-engineered H1N1 A/PuertoRico/8/34 virus, after four MDCK cell passages, possessed greater heterogeneity in shape than the uniformly spherical A/NewCaledonia/20/99(H1N1), with a relatively higher percentage of elongated viruses, similar to observations previously described with early egg-passaged human influenza viruses (Choppin et al., 1960). The various PR8-Moscow/10 recombinant viruses presented a heterogeneous pattern of shapes and there was no apparent correlation with genetic composition, inconsistent with subtype-specific differences.

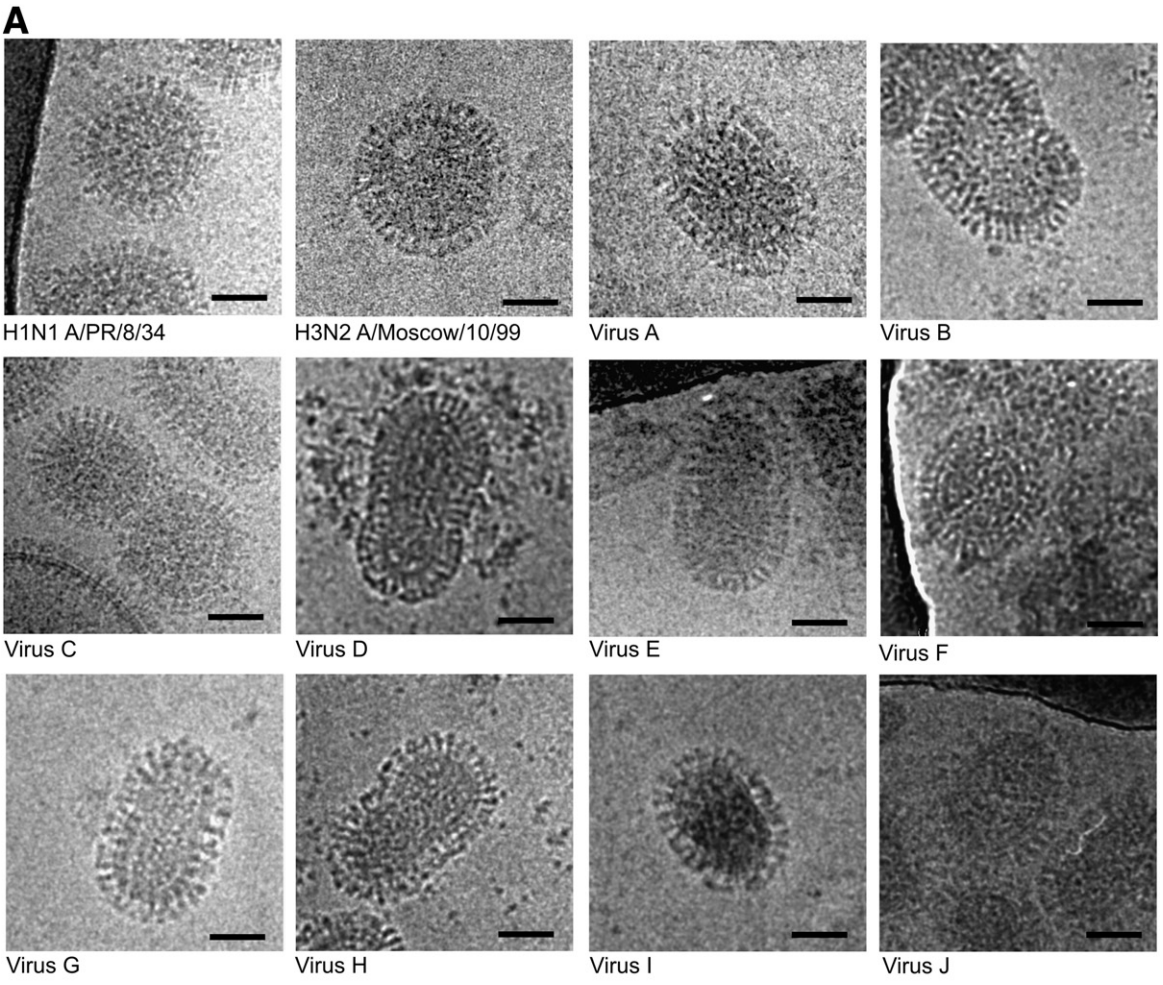
A
H1N1 A/PR/8/34
H3N2 A/Moscow/10/99
Virus A
Virus B
Virus C
Virus D
Virus E
Virus F
Virus G
Virus H
Virus I
Virus J

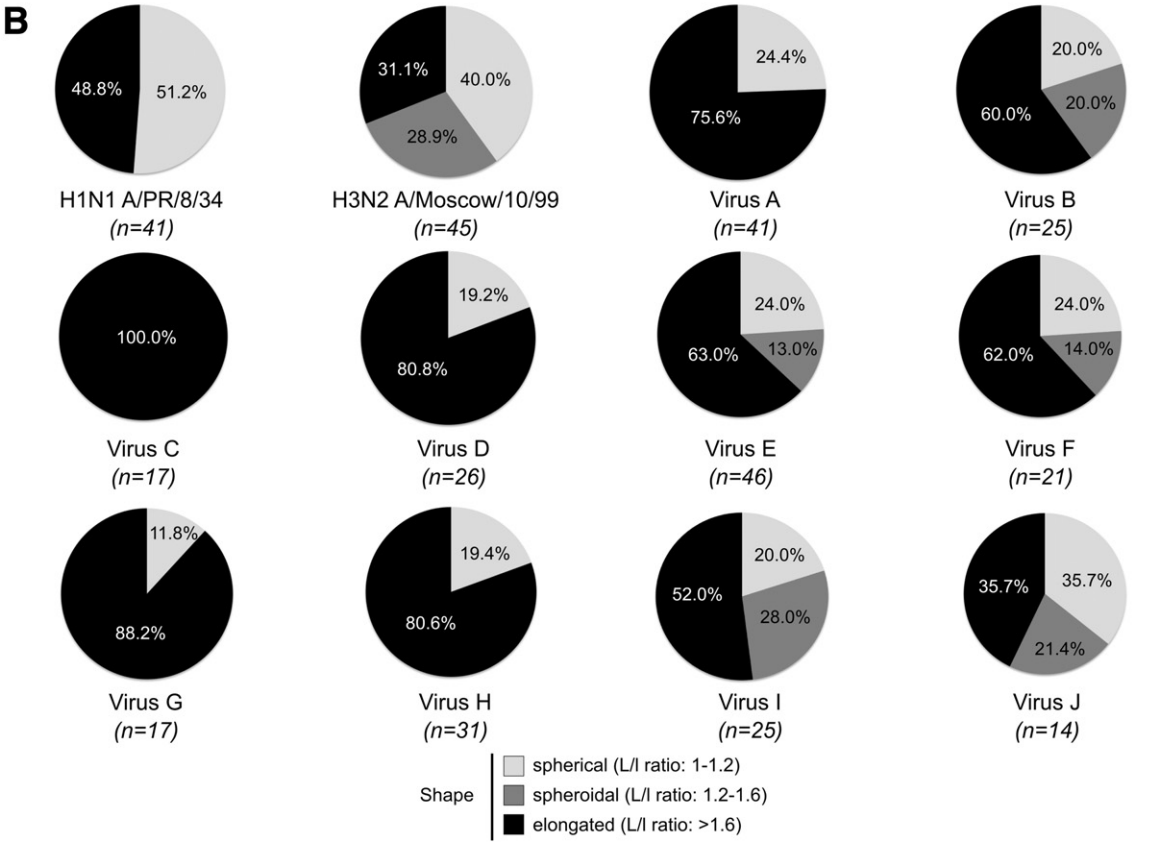
B
48.8%
51.2%
H1N1 A/PR/8/34
(n=41)
31.1%
40.0%
28.9%
H3N2 A/Moscow/10/99
(n=45)
24.4%
75.6%
Virus A
(n=41)
20.0%
60.0%
20.0%
Virus B
(n=25)
100.0%
Virus C
(n=17)
19.2%
80.8%
Virus D
(n=26)
24.0%
63.0%
13.0%
Virus E
(n=46)
24.0%
62.0%
14.0%
Virus F
(n=21)
11.8%
88.2%
Virus G
(n=17)
19.4%
80.6%
Virus H
(n=31)
20.0%
52.0%
28.0%
Virus I
(n=25)
35.7%
35.7%
21.4%
Virus J
(n=14)
Shape
spherical (L/l ratio: 1-1.2)
spheroidal (L/l ratio: 1.2-1.6)
elongated (L/l ratio: >1.6)

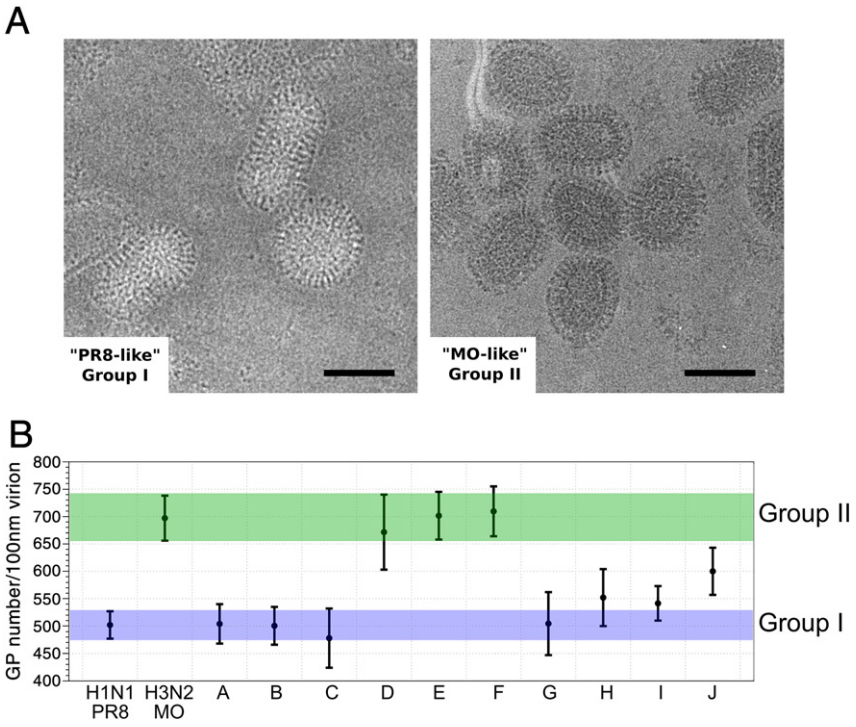

Fig. 4. A. Representative micrographs of ice-embedded "PR8-like" and "MO-like" viruses (respectively, groups I and II), scale bar 100 nm. B. Comparison of the estimated GP number per 100 nm diameter virion for A/PR/8/34(H1N1), A/Moscow/10/99(H3N2) and 10 recombinant viruses. Groups I and II are respectively highlighted in blue and green.

Our estimations of the total number of surface GP spikes for both H1N1 and H3N2 viruses was higher than previously described in the literature. The available data on surface GP number have largely been obtained for egg-passaged viruses. We therefore examined an egg-passaged H3N2 virus A/Panama/2007/99 and estimated the GP number range to be 458–513 for an average 100 nm diameter virion, that was closer to the previous observations of 350–500 GPs obtained from earlier biochemical studies (Inglis et al., 1976). However, after 4 passages on MDCK cells, the same H3N2 strain harboured around 24% more GPs at the surface, a level similar to those of the MDCK cell-grown A/California/7/04(H3N2) and recombinant MO viruses. The marked differences observed between egg- and MDCK cell-passaged A/Panama/2007/99(H3N2) viruses emphasise once again the major influence of cell substrate both on morphology and GP density, although the mechanism of host determinants of virus morphology remains largely unknown.

Since the two GPs are anchored in lipid rafts (Kundu et al., 1996; Scheiffele et al., 1997; Scheiffele et al., 1997) and because of the possible role of lipid rafts in the regulation of bud closing and bud release steps (Barman and Nayak, 2007), it is possible that differences in lipid composition between MDCK and chicken egg allantoic membrane cells impact the spatial organisation of the virus envelope. The relative versatility in shape between the same or different subtypes, illustrated well by all the recent observations of fully hydrated influenza virions, including ours, could be related to the intrinsic versatility of the cytoskeleton, as previously shown by actin microfilament inhibition experiments (Roberts and Compans, 1998). Interestingly, the link between actin cytoskeleton, lipid rafts and influenza virion morphology has been demonstrated previously by Simpson-Holley et al. (2002). Moreover, even using similar virus production, the same cell system and culture conditions, we cannot exclude possible roles for cellular determinants, reflected in differential responses to infection. Altogether, these results reveal a complex role for host components in determining both the surface GP organisation and the shape of the influenza virus.

The estimates of total surface GP were highly reproducible among the genetic-engineered and natural viruses and provided the basis for investigation of the virus-specific determinants of this feature of virus morphology using cryo-EM in conjunction with reverse genetics. To limit the number of recombinant viruses with different genetic makeups for this cryo-EM study, we chose to focus on the impact of variation in MO gene segments on a PR8 genetic background. Via their interactions with lipid rafts, the surface GPs are thought to be an essential factor in morphogenesis (Nayak et al., 2009). To explore their role in determining GP surface density we constructed a "6 + 2" recombinant (virus A, Fig. 2) containing both H3 and N2 gene segments from MO in the PR8 genetic background. This typical vaccine virus was shown to harbour a similar number of GPs to that estimated for the PR8 recombinant virus. Harris et al. have shown that the number of GP spikes on the surface of the egg-produced recombinant X31, comprising the HA and NA gene segments of A/Hong Kong/68 (H3N2) in a PR8 genetic background (Baez et al., 1980), was approximately 340 spikes for a 120 nm average diameter virion (Harris et al., 2006). Considering that egg production may cause a decrease of the order of 24% in GP on the virus surface, our data appear comparable to the cryo-ET study by Harris et al. Similar GP densities were observed for "7 + 1" recombinant viruses containing HA or NA MO coding sequences (viruses G and H). Thus the GP genes alone are

Fig. 3. Comparison of morphological features of the 12 recombinant viruses obtained by reverse genetic, by cryo-electron microscopy (part I). A. Representative micrographs of ice embedded virions of A/PR/8/34(H1N1 PR8) and A/Moscow/10/99(H3N2 MO), and 10 different recombinant viruses grown in MDCK cells. The genome compositions of each virus are given in Fig. 2. Scale bars: 50 nm. B. Proportions of the different shapes observed for the 12 different viruses, the total number of virions analysed for each virus is indicated in brackets.

A

Viruses	GP spikes	
	4 GP spacing (average +/- SD, nm)	GP/ 100nm spherical virion (range, nm)
H1N1 A/PR/8/34 (RG)	**31.7** +/- 0.8 *(n=62)*	**[477 - 527]**
H3N2 A/Moscow/10/99 (RG)	**26.9** +/- 0.8 *(n=79)*	**[656 - 738]**
Virus A	**31.6** +/- 1.1 *(n=78)*	**[468 - 540]**
Virus B	**31.7** +/- 1.1 *(n=84)*	**[465 - 536]**
Virus C	**32.6** +/- 1.8 *(n=47)*	**[424 - 532]**
Virus D	**27.5** +/- 1.4 *(n=119)*	**[603 - 740]**
Virus E	**26.8** +/- 0.8 *(n=33)*	**[658 - 745]**
Virus F	**26.7** +/- 0.9 *(n=98)*	**[664 - 755]**
Virus G	**31.7** +/- 1.8 *(n=42)*	**[447 - 562]**
Virus H	**30.3** +/- 1.4 *(n=111)*	**[500 - 604]**
Virus I	**30.5** +/- 0.9 *(n=70)*	**[510 - 573]**
Virus J	**29.0** +/- 1.0 *(n=52)*	**[557 - 643]**

B

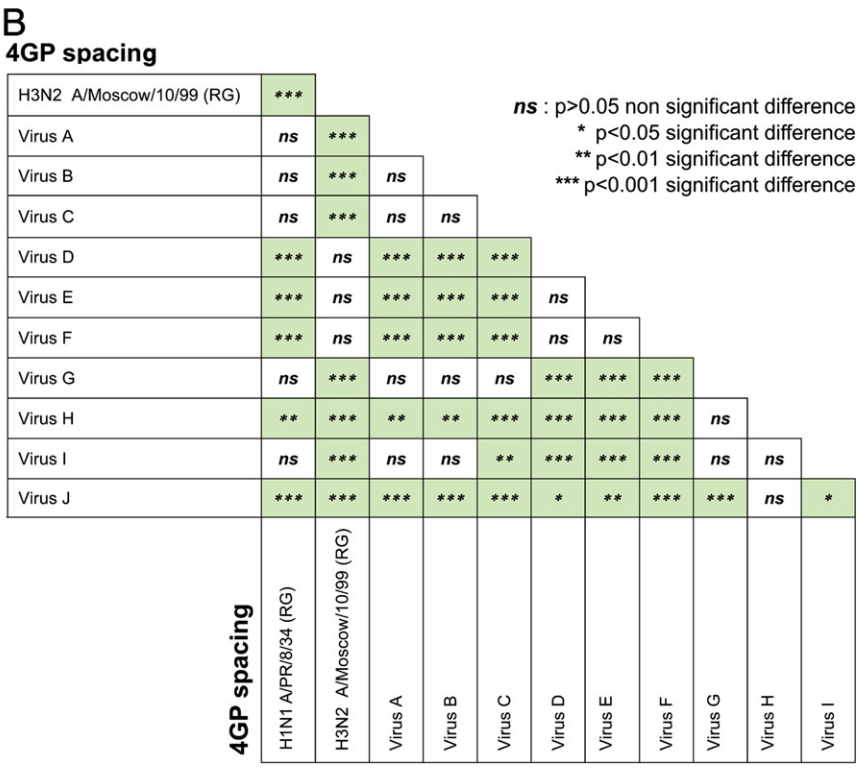

Fig. 5. Comparison of morphological features of the 12 recombinant viruses. A. Measure of the 4GP spacing for each virus and determination of the surface GP range per 100 nm diameter virion. An example of the calculation is given in Supplementary Fig. 2. B. Dunn's multiple comparisons test, after a non-parametric ANOVA (Kruskal–Wallis test). Statistical analysis was based on 4GP-spacing data obtained from the 12 different viruses.

not responsible for the marked difference in surface GP density between H1N1 and H3N2 parental viruses. Furthermore, additional substitution of MO M or NS gene segments did not influence the specific GP density. Only recombinants containing PB1 or PB2 MO coding sequences in addition to HA presented a similar GP density to that observed for the MO recombinant virus. Recently, Li et al. (2010) showed that the introduction of the PB2 from a human H3N2 strain into reassortant viruses containing H5N1 gene segments is crucial for obtaining highly pathogenic reassortant viruses. That study suggested that the human virus PB2 protein may be responsible for efficient transmission of pandemic viruses among humans by conferring efficient growth at the lower temperature of the upper respiratory tract. Our results raise the possibility that the human virus PB2 protein might also modulate the GP density of highly pathogenic reassortant viruses.

Although our results indicate that the genomic composition has a significant impact on the surface GP density, its possible effect on the HA/NA ratio remains to be investigated. Theoretical calculations from biochemical studies indicate around 4 fold more HA than NA (HA/NA ratio = 4) (Inglis et al., 1976). Hausmann et al. (1997) have shown that a marked difference between HA and NA in rates of intracellular transport to the plasma membrane may contribute towards the greater abundance of HA in the viral envelope. More recent observations by cryo-ET (Harris et al., 2006) suggest a higher ratio, around 6 to 8. In our cryo-EM micrographs, it was not possible to easily discriminate NA from HA on the virion surface. We therefore

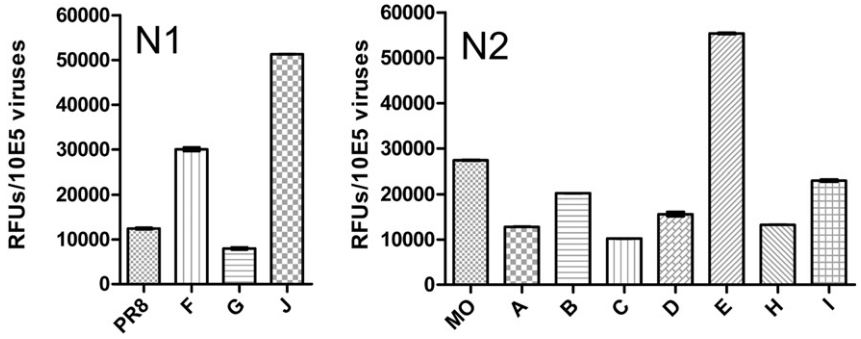

Fig. 6. Comparison of NA activities (RFUs) of recombinant viruses. NA activities were measured using the MUNANA substrate and are shown as RFU values for 10^5 TCID50. Comparison of influenza NA activities of N1 or N2 viruses differing from each other by internal and/or HA genes. Viruses differing from each other only by internal genes.

estimated the amount of NA in virus preparations by measuring the NA activities (RFU) of recombinant viruses harbouring the same NA and used this as a measure of NA molecules incorporated into virus. In the case of equivalent GP surface densities, differences in NA activity suggest modification of the HA/NA ratio. It was apparent from comparisons of viruses differing only in PB1 that substitution of PR8 PB1 by that of MO resulted in increases in NA activity which correlated with increases in GP density. Recently, Wanitchang et al. (2010) have shown that the NA activity of genetic-engineered «5 + 3» viruses containing the HA, NA and PB1 gene segments of the novel 'swine-origin' H1N1 influenza virus in the genetic background of PR8 was higher than that of the genetic-engineered "6 + 2" virus. A possible bias in the analysis may relate to differences in the proportions of different shapes between viruses; the elongated forms potentially possessing a higher number of surface GPs. However, this bias seemed to be reduced when comparing the different levels of NA activity measured for recombinants D, E and F despite their similar surface GP densities and shape proportions (Figs. 3B, 4B and 5A). Precise measurements of ratios of NA to HA molecules on virions, in relation to genetic composition, will however require direct quantitation, for example using cryo-ET.

No marked changes were observed in the production of infectious virus in MDCK cells; however, differences were observed in the replication of some recombinants in MDCK-SIAT1 cells. It is well established that MDCK-SIAT1 cells prove to be a more suitable system than MDCK cells to monitor the impact of modulation of the functional HA/NA balance during the growth process (Matrosovich et al., 2003; Moules et al., 2010). A heterologous MO PB1 or PB2 polymerase component was associated with reduced production of infectious H3 viruses in MDCK-SIAT1 cells, possibly due to changes in the HA/NA ratio at the viral surface and the HA/NA functional balance, whereas the MO PB1 did not affect the growth of PR8 H1 recombinant viruses (the HA of which has dual specificity for binding α(2,3)- and α(2,6)-linked sialic acids). For more definitive conclusions, however, further experiments are necessary to investigate the binding properties of the HA in relation to NA activity of the different recombinant viruses.

These results serve to emphasize the complexities underlying the interactions between virus and host determinants in modulating the progress and outcome of influenza infection.

Together, the results of these experiments have emphasized an important contribution of the polymerase constitution to various aspects of the replication and assembly of the virus and in particular a potential important functional link between PB1 and HA. This conclusion is reinforced by the genomic compositions of the 1957 and 1968 pandemic viruses, which incorporated PB1 in addition to HA and NA or HA avian gene segments, respectively (Kawaoka et al., 1989). Furthermore, Tumpey et al. (2005) have shown that both HA and polymerase gene segments of recombinant 1918 pandemic H1N1 viruses are essential for maximum replication in human bronchial epithelial cells and consequently its extreme virulence. In the emergence of recombinant viruses through genetic reassortment, PB1-linked modulation of GP production and incorporation into virus may play a role in modulating the HA/NA functional balance important in the interplay between NA and HA for the replicative efficiency of influenza viruses. In this respect, we have recently demonstrated a putative functional link between HA proteins and PB1 gene products in the context of the emergence of NA inhibitor-resistant H3 viruses lacking the NA gene segment, the mechanism of which has yet to be elucidated (Moules et al., 2010).

From a practical perspective, the influence on virus morphology and density of HA and NA glycoproteins on the virus surface might be exploited in the development by reverse genetics of recombinant viruses with enhanced growth and HA (and NA) content for increased vaccine production.

Materials and methods

Cells and viruses

Madin–Darby Canine Kidney (MDCK) cells were purchased from Cambrex Bioscience (ATCC, CCL34), Walkersville, Md. Cells were passaged twice weekly in serum free Ultra-MDCK medium (Cambrex Bioscience) supplemented with 2 mM L-glutamine (Sigma Aldrich, St. Louis, Mo.), penicillin (225 U/mL) and streptomycin (225 μg/mL) (Cambrex Bioscience, Walkersville, Md). A549 cells were maintained in Dulbecco's modified Eagle's medium supplemented with 10% foetal calf serum and supplemented with 2 mM L-glutamine (Sigma Aldrich, St.Louis, Mo.), penicillin (225 U/mL) and streptomycin (225 μg/mL) (Cambrex Bioscience, Walkersville, Md). All cells were maintained at 37 °C with 5% CO2. Vaccine prototype egg-adapted viruses (2 passages) were adapted to cell culture four by successive passages on MDCK cells (MOI 0.001 to 0.00001).

Cryo-electron microscopy

In order to preserve, as much as possible, intact viral particles, we choose to avoid several purification/concentrations steps by saccharose gradient and/or ultracentrifugation. With the same objective, the cryo-EM technique has the advantage of not using negative stains, which are thought to introduce possible artefact in the shape, size and morphology of virus particles (Ruigrok et al., 1992; Terrier et al., 2009). For cryo-EM, four microlitres of sample were loaded onto a Quantifoil R2/1 holey grid (Quantifoil Micro Tools GmbH, Germany), blotted for 1 to 2 seconds to remove the excess liquid and then rapidly plunged into liquid ethane cooled using liquid nitrogen. The frozen grid was transferred into a LaB6 CM200 Philips electron microscope using a GATAN 626 cryoholder. The images were taken under low dose conditions at 200 kV (less than 10 $e^-/Å^2$) and with a nominal magnification of 38,000 and a defocus between 2 and 3 μm either on

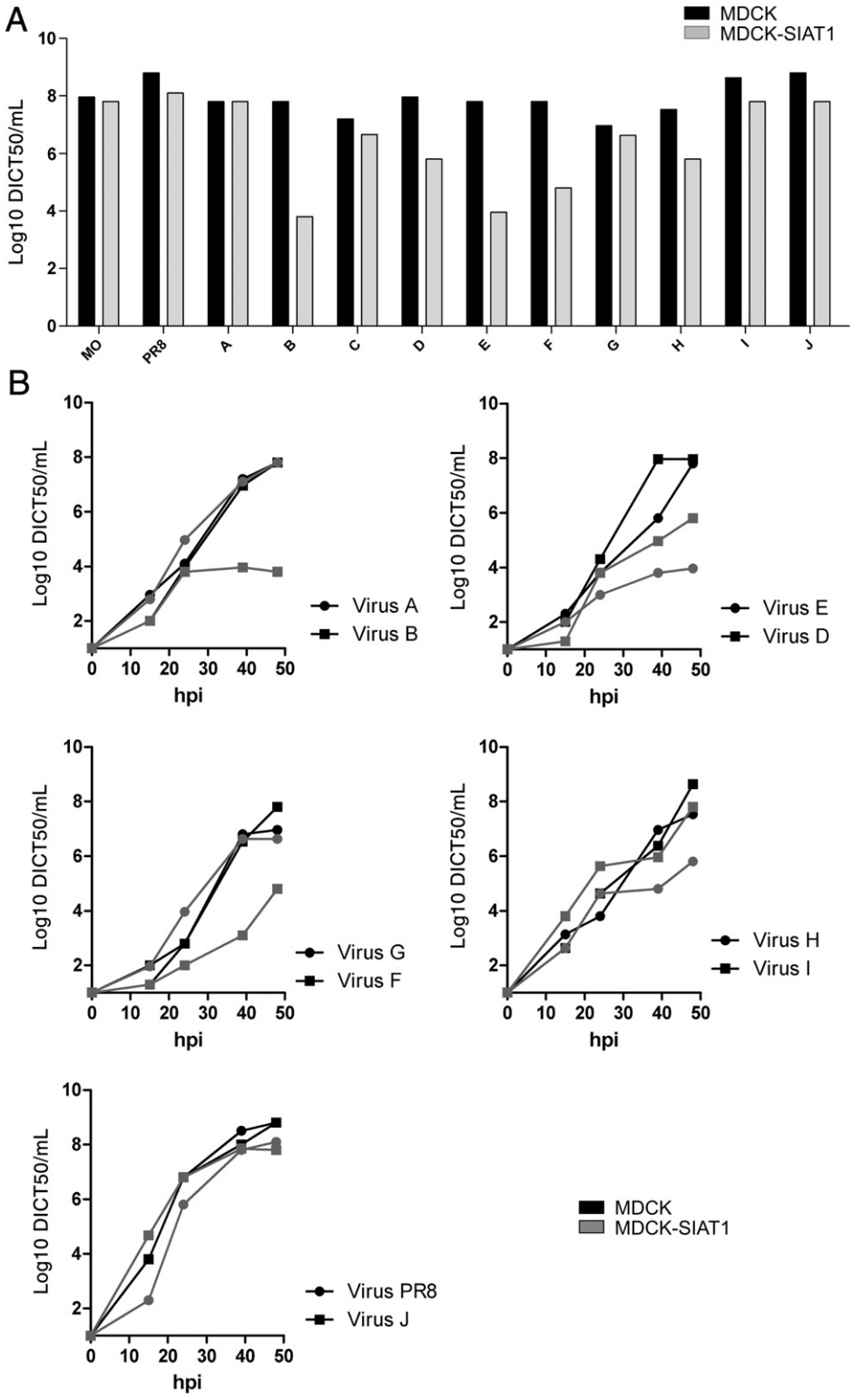

Fig. 7. Kinetics of replication of recombinant viruses in MDCK and MDCK-SIAT1 cells. A. Viral titers of recombinant viruses at 48 hpi in MDCK and MDCK-SIAT1 cells. B. Kinetics of replication of recombinant viruses in MDCK and MDCK-SIAT1 cells (MOI of 10^{-4}).

film or using a CCD camera (GATAN ultrascan 1000). The negatives were developed in full strength D19 developer for 12 min. Negatives were digitised using the Photoscan TD with a pixel size of 14 mm (3.5 Å per pixel at the specimen level for film and for the CCD camera as calibrated using Tobacco Mosaic Virus).

Measures and statistical analysis

Different viral structures were measured and calculated (diameter, GP spikes length, GP spikes surface density Fig. 3C) on the Cryo-EM micrographs, with the help of the ImageJ software (http://rsbweb.nih.

gov/ij/). The GP spikes surface density was calculated as described previously (Yamaguchi et al., 2008). The methodology and an example of calculation are shown in Supplementary data 2. Surface density data were subjected to statistical analysis by using the Instat 3 Graphpad software. A Kruskal–Wallis test (non-parametric ANOVA) followed by a Dunn's multiple comparison test were performed. Statistical significance was accepted at the probability level of $p<0.05$, $p<0.01$ or $p<0.001$.

NA activity assays

The neuraminidase activity was determined by a fluorometric assay as described previously (Ferraris et al., 2005). A volume of 50 µl of diluted viruses (2.10E3 TCID50/µl) viruses was incubated with 50 µl of 200 µM 2-(4-methylumbelliferyl)-alpha-D-N-acetylneuraminic acid (4-MUNANA) substrate (Sigma) at 37 °C for 1 h. The enzymatic reaction was stopped by the addition of 150 µl of 50 mM glycine (pH 10.4). The fluorescence level of the released 4-methylumbelliferone was determined at an excitation wavelength of 355 nm and an emission wavelength of 460 nm with a BMG Labtek fluorometer.

Reverse genetic systems

A/PR/8/34, A/Moscow/10/99 and all reassortants viruses were generated by reverse genetic as previously described (Hoffmann et al., 2000). Briefly, viral RNA was extracted by using QIAmp viral RNA minikit (Qiagen) from infected-MDCK cell culture supernatant, according to the manufacturer's instructions. Two-step RT-PCR was carried out for full-length amplification of each viral RNA gene segment, by using influenza A universal RT primers (Uni-12primer«3′-AGCAAAAGCAGG-5′ », Eurogentec, Belgium) as previously described. The cDNA obtained from the different genes were cloned into the pHW2000 vector (Hoffmann et al., 2000) allowing expression of both corresponding vRNAs and viral proteins. Recombinant viruses were generated by DNA transfection. Plasmids were mixed with Superfect reagent (Qiagen) in Opti-MEM (GIBCO-BRL), according to the manufacturer's instructions and added to 293 T cells in six-well tissue culture plates. At 48 h post-transfection, viruses in the culture supernatant were harvested and used to infect MDCK cells to be amplified. After two passages on MDCK cells, titers were measured using standard methods.

Viral growth kinetics and end point titration

MDCK cells were infected at a multiplicity of infection (MOI) of 10^4 TCID50/cell. After a 1-h viral adsorption period, cells were overlaid with Eagle's minimum elementary medium (EMEM, Lonza) supplemented with 1 µg/ml trypsin (Roche diagnostics) and further incubated at 34 °C. Harvested supernatants were centrifuged at 1500*g* for 10 min and stored at −70 °C until analysis. End point-titration assays were performed on confluent layers of MDCK cells in 96-well plates. Briefly, 50 µl of 10-fold serial dilutions of each virus was inoculated into four replicate wells. The 96-well microplates were incubated at 34 °C and the presence of cytopathic effects (CPE) was monitored 3 days later under the microscope. The presence of virus in supernatants was also confirmed by haemagglutination tests using guinea pig erythrocytes. The TCID50 per ml values were determined using the Reed and Muench statistical method.

Supplementary materials related to this article can be found online at doi:10.1016/j.virol.2011.03.011.

Acknowledgments

We are grateful to Dr H.D. Klenk and Dr M. Matrosovich (Institute Virology, Marburg, Germany) for providing the MDCK-SIAT1 cells. We also wish to thank Dr N. Naffakh (Institut Pasteur, Paris) for the helpful discussion. This project was supported by the "Maladies Infectieuses Emergentes" programme from the CNRS.

References

Baez, M., Palese, P., Kilbourne, E.D., 1980. Gene composition of high-yielding influenza vaccine strains obtained by recombination. J. Infect. Dis. 141 (3), 362–365 Mar.
Barman, S., Nayak, D.P., 2007. Lipid raft disruption by cholesterol depletion enhances influenza A virus budding from MDCK cells. J. Virol. 81 (22), 12169–12178 Nov.
Booy, F.P., Ruigrok, R.W., van Bruggen, E.F., 1985. Electron microscopy of influenza virus. A comparison of negatively stained and ice-embedded particles. J. Mol. Biol. 184 (4), 667–676 Aug 20.
Calder, L.J., Wasilewski, S., Berriman, J.A., Rosenthal, P.B., 2010. Structural organization of a filamentous influenza A virus. Proc. Natl Acad. Sci. U.S.A. 107 (23), 10685–10690 Jun 8.
Choppin, P.W., Murphy, J.S., Tamm, I., 1960. Studies of two kinds of virus particles which comprise influenza A2 virus strains. III. Morphological characteristics: independence to morphological and functional traits. J. Exp. Med. 112, 945–952 Nov 1.
Eichelberger, M.C., Hassantoufighi, A., Wu, M., Li, M., 2008. Neuraminidase activity provides a practical read-out for a high throughput influenza antiviral screening assay. Virol. J. 5, 109 Sep 26.
Ferraris, O., Kessler, N., Lina, B., 2005. Sensitivity of influenza viruses to zanamivir and oseltamivir: a study performed on viruses circulating in France prior to the introduction of neuraminidase inhibitors in clinical practice. Antivir. Res. 68 (1), 43–48 Oct.
Fujiyoshi, Y., Kume, N.P., Sakata, K., Sato, S.B., 1994. Fine structure of influenza A virus observed by electron cryo-microscopy. EMBO J. 13 (2), 318–326 Jan 15.
Gong, J., Xu, W., Zhang, J., 2007. Structure and functions of influenza virus neuraminidase. Curr. Med. Chem. 14 (1), 113–122.
Gubareva, L.V., Bethell, R., Hart, G.J., Murti, K.G., Penn, C.R., et al., 1996. Characterization of mutants of influenza A virus selected with the neuraminidase inhibitor 4-guanidino-Neu5Ac2en. J. Virol. 70 (3), 1818–1827 Mar.
Harris, A., Cardone, G., Winkler, D.C., Heymann, J.B., Brecher, M., et al., 2006. Influenza virus pleiomorphy characterized by cryoelectron tomography. Proc. Natl Acad. Sci. U.S.A. 103 (50), 19123–19127 Dec 12.
Hausmann, J., Kretzschmar, E., Garten, W., Klenk, H.D., 1997. Biosynthesis, intracellular transport and enzymatic activity of an avian influenza A virus neuraminidase: role of unpaired cysteines and individual oligosaccharides. J. Gen. Virol. 78 (Pt 12), 3233–3245 Dec.
Hayase, Y., Uno, F., Nii, S., 1995. Ultrahigh-resolution scanning electron microscopy of MDCK cells infected with influenza viruses. J. Electron. Microsc. (Tokyo.) 44 (5), 281–288 Oct.
Hoffmann, E., Neumann, G., Kawaoka, Y., Hobom, G., Webster, R.G., 2000. A DNA transfection system for generation of influenza A virus from eight plasmids. Proc. Natl Acad. Sci. U.S.A. 97 (11), 6108–6113 May 23.
Huiskonen, J.T., Overby, A.K., Weber, F., Grünewald, K., 2009. Electron cryo-microscopy and single-particle averaging of Rift Valley fever virus: evidence for GN-GC glycoprotein heterodimers. J. Virol. 83 (8), 3762–3769 Apr.
Inglis, S.C., Carroll, A.R., Lamb, R.A., Mahy, B.W., 1976. Polypeptides specified by the influenza virus genome I. Evidence for eight distinct gene products specified by fowl plague virus. Virology 74 (2), 489–503 Oct 15.
Kawaoka, Y., Krauss, S., Webster, R.G., 1989. Avian-to-human transmission of the PB1 gene of influenza A viruses in the 1957 and 1968 pandemics. J. Virol. 63 (11), 4603–4608 Nov.
Kundu, A., Avalos, R.T., Sanderson, C.M., Nayak, D.P., 1996. Transmembrane domain of influenza virus neuraminidase, a type II protein, possesses an apical sorting signal in polarized MDCK cells. J. Virol. 70 (9), 6508–6515 Sep.
Lamb, R.A., Krug, R.M., 2001. In: Knipe, D.M., Howley, P.M. (Eds.), Fields Virology, 1. Lippincott Williams and Wilkins, New York, pp. 1487–1579.
Li, C., Hatta, M., Nidom, C.A., Muramoto, Y., Watanabe, S., et al., 2010. Reassortment between avian H5N1 and human H3N2 influenza viruses creates hybrid viruses with substantial virulence. Proc. Natl Acad. Sci. U.S.A. 107 (10), 4687–4692 Mar 9.
Loney, C., Mottet-Osman, G., Roux, L., Bhella, D., 2009. Paramyxovirus ultrastructure and genome packaging: cryo-electron tomography of sendai virus. J. Virol. 83 (16), 8191–8197 Aug.
Matrosovich, M., Matrosovich, T., Carr, J., Roberts, N.A., Klenk, H.D., 2003. Overexpression of the alpha-2,6-sialyltransferase in MDCK cells increases influenza virus sensitivity to neuraminidase inhibitors. J. Virol. 77 (15), 8418–8425 Aug.
McKimm-Breschkin, J.L., McDonald, M., Blick, T.J., Colman, P.M., 1996. Mutation in the influenza virus neuraminidase gene resulting in decreased sensitivity to the neuraminidase inhibitor 4-guanidino-Neu5Ac2en leads to instability of the enzyme. Virology 225 (1), 240–242 Nov 1.
Moules, V., Ferraris, O., Terrier, O., Giudice, E., Yver, M., et al., 2010. In vitro characterization of naturally occurring influenza H3NA- viruses lacking the NA gene segment: toward a new mechanism of viral resistance? Virology 404 (2), 215–224 Sep 1.
Nayak, D.P., Reichl, U., 2004. Neuraminidase activity assays for monitoring MDCK cell culture derived influenza virus. J. Virol. Meth. 122 (1), 9–15 Dec 1.
Nayak, D.P., Balogun, R.A., Yamada, H., Zhou, Z.H., Barman, S., 2009. Influenza virus morphogenesis and budding. Virus Res. 143 (2), 147–161 Aug.
Neumann, G., Noda, T., Kawaoka, Y., 2009. Emergence and pandemic potential of swine-origin H1N1 influenza virus. Nature 459 (7249), 931–939 Jun 18.
Noda, T., Sagara, H., Yen, A., Takada, A., Kida, H., et al., 2006. Architecture of ribonucleoprotein complexes in influenza A virus particles. Nature 439 (7075), 490–492 Jan 26.

Palese, P., Shaw, M.L., 2007. *Orthomyxoviridae*: the viruses and their replication, In: Knipe, D.M., Howley, P.M., Griffi, D.E., Lamb, R.A., Martin, M.A., Roizman, B., Strauss, S.E. (Eds.), Fields Virology, 5th edition. Lippincott Williams and Wilkins, Philadelphia, pp. 1647–1689.

Roberts, P.C., Compans, R.W., 1998. Host cell dependence of viral morphology. Proc. Natl Acad. Sci. U.S.A. 95 (10), 5746–5751 May 12.

Ruigrok, R.W., Andree, P.J., Hooft van Huysduynen, R.A., Mellema, J.E., 1984. Characterization of three highly purified influenza virus strains by electron microscopy. J. Gen. Virol. 65 (Pt 4), 799–802 Apr.

Ruigrok, R.W., Hewat, E.A., Wade, R.H., 1992. Low pH deforms the influenza virus envelope. J. Gen. Virol. 73 (Pt 4), 995–998 Apr.

Scheiffele, P., Roth, M.G., Simons, K., 1997. Interaction of influenza virus haemagglutinin with sphingolipid–cholesterol membrane domains via its transmembrane domain. EMBO J. 16 (18), 5501–5508 Sep 15.

Sherman, M.B., Freiberg, A.N., Holbrook, M.R., Watowich, S.J., 2009. Single-particle cryo-electron microscopy of Rift Valley fever virus. Virology 387 (1), 11–15 Apr 25.

Simpson-Holley, M., Ellis, D., Fisher, D., Elton, D., McCauley, J., et al., 2002. A functional link between the actin cytoskeleton and lipid rafts during budding of filamentous influenza virions. Virology 301 (2), 212–225 Sep 30.

Skehel, J.J., Wiley, D.C., 2002. Influenza haemagglutinin. Vaccine 20 (Suppl 2), S51–S54 May 15.

Staschke, K.A., Colacino, J.M., Baxter, A.J., Air, G.M., Bansal, A., et al., 1995. Molecular basis for the resistance of influenza viruses to 4-guanidino-Neu5Ac2en. Virology 214 (2), 642–646 Dec 20.

Terrier, O., Rolland, J.P., Rosa-Calatrava, M., Lina, B., Thomas, D., et al., 2009. Parainfluenza virus type 5 (PIV-5) morphology revealed by cryo-electron microscopy. Virus Res. 142 (1–2), 200–203 Jun.

Tumpey, T.M., Basler, C.F., Aguilar, P.V., Zeng, H., Solorzano, A., et al., 2005. Characterization of the reconstructed 1918 Spanish influenza pandemic virus. Science 310 (5745), 77–80 Oct 7.

Wanitchang, A., Kramyu, J., Jongkaewwattana, A., 2010. Enhancement of reverse genetics-derived swine-origin H1N1 influenza virus seed vaccine growth by inclusion of indigenous polymerase PB1 protein. Virus Res. 147 (1), 145–148 Jan.

Yamaguchi, M., Danev, R., Nishiyama, K., Sugawara, K., Nagayama, K., 2008. Zernike phase contrast electron microscopy of ice-embedded influenza A virus. J. Struct. Biol. 162 (2), 271–276 May.

Zhang, J., Pekosz, A., Lamb, R.A., 2000. Influenza virus assembly and lipid raft microdomains: a role for the cytoplasmic tails of the spike glycoproteins. J. Virol. 74 (10), 4634–4644 May.